Atmos. Meas. Tech., 6, 387–396, 2013
www.atmos-meas-tech.net/6/387/2013/
doi:10.5194/amt-6-387-2013

Atmospheric Measurement Techniques
Open Access

An airborne amplitude-modulated 1.57 µm differential laser absorption spectrometer: simultaneous measurement of partial column-averaged dry air mixing ratio of CO_2 and target range

D. Sakaizawa[1], S. Kawakami[1], M. Nakajima[1], T. Tanaka[2,*], I. Morino[2], and O. Uchino[2]

[1]Japan Aerospace Exploration Agency (JAXA), Tsukuba, Japan
[2]National Institute for Environmental Studies, Tsukuba, Japan
[*]now at: Japan Aerospace Exploration Agency, Tsukuba, Japan

Correspondence to: D. Sakaizawa (sakaizawa.daisuke@jaxa.jp)

Received: 12 May 2012 – Published in Atmos. Meas. Tech. Discuss.: 13 July 2012
Revised: 10 December 2012 – Accepted: 4 January 2013 – Published: 19 February 2013

Abstract. Simultaneous measurements of the partial column-averaged dry air mixing ratio of CO_2 (XCO_2) and target range were demonstrated using airborne amplitude-modulated 1.57 µm differential laser absorption spectrometer (LAS). The LAS system is useful for discriminating between ground and cloud return signals and has a demonstrated ability to suppress the impact of integrated aerosol signals on atmospheric CO_2 measurements. A high correlation coefficient (R) of 0.987 between XCO_2 observed by LAS and XCO_2 calculated from in situ measurements was obtained. The averaged difference in XCO_2 obtained from LAS and validation data was within 1.5 ppm for all spiral measurements. An interesting vertical profile was observed for both XCO_{2LAS} and XCO_{2val}, in which lower altitude CO_2 decreases compared to higher altitude CO_2 attributed to the photosynthesis over grassland in the summer. In the case of an urban area where there are boundary-layer enhanced CO_2 and aerosol in the winter, the difference of XCO_{2LAS} to XCO_{2val} is a negative bias of 1.5 ppm, and XCO_{2LAS} is in agreement with XCO_{2val} within the measurement precision of 2.4 ppm (1 SD).

1 Introduction

Evaluation of the spatial and temporal distribution of natural carbon fluxes over land and ocean continues to be difficult, hindering improvements in the quantification and understanding of the mechanism of the fluxes (Kawa et al., 2010; Kaminske et al., 2010). Uncertainty in flux evaluations is a major contributor to uncertainty in climate predictions (Randall et al., 2007). However, confirmation of the consistency between the sum of the regional and global budgets of carbon fluxes is expected to provide a unique index of the level of confidence in the outcomes of climate mitigation policies (IPCC, 2007). A global carbon cycle study using higher spatial resolution than an $8° \times 10°$ grid is currently required to improve the knowledge of the carbon cycle (Rayner and O'Brien, 2001; Baker et al., 2011). Transport models and observational data sets improve evaluations of regional carbon fluxes (Maksyutov et al., 2008). A sustainable technique for CO_2 remote sensing from space is one of the greatest challenges and necessities for understanding the global carbon cycle, as well as for predicting and validating its evolution under future climate changes.

The Greenhouse gases Observing SATellite (GOSAT) is the first step in dealing with the above-mentioned issue (Kuze et al., 2009; Yoshida et al., 2011; Palmer et al., 2011). The sensors on-board GOSAT are based on a passive remote sensing technique. The GOSAT sensor was developed to derive the column-averaged mixing ratio of CO_2 (XCO_2) with a precision better than 1 % for an $8° \times 10°$ grid without any biases or with uniform bias (Rayner and O'Brien, 2001; Houweling et al., 2004; Miller et al., 2007; Morino et al., 2011). However, there are unavoidable limitations imposed by the measurement approach: (1) the best performance for CO_2 total column measurements can only be obtained under clear-sky conditions; (2) seasonal dependence, such as in the

case of the Northern Hemisphere in winter, reduces its global coverage; and (3) CO_2 measurements are highly sensitive to unknowns and variations in cloud and aerosol contamination.

In contrast, active optical remote sensing techniques as a differential absorption spectrometer (LAS) are less impacted by the above factors on atmospheric CO_2 measurements. Ground-based differential absorption lidar (DIAL) using a high-energy pulse laser has been developed to measure vertical CO_2 mixing ratios (Amediek et al., 2008; Sakaizawa et al., 2009; Ishii et al., 2010; Gibert et al., 2011). Airborne systems to observe partial column-averaged CO_2 have also been reported in earlier studies (Browell et al., 2011; Abshire et al., 2010; Spiers et al., 2011) to demonstrate technology feasible for future space-borne missions. Although in a pulsed system aerosol or cirrus clouds have less impact on total column measurements, the pulsed-laser wavelength must be stabilized at a seeding laser wavelength with a precision of less than 100 kHz to reduce error due to wavelength stability, which requires large resources. Errors due to variations in the surface reflectivity along the track also increase the impact, unless the transmitter has a double pulse system (Yu et al., 2003). Our fiber-based continuous laser approach to measure the differential absorption optical depth (DAOD = $\Delta\tau$) allows for compact storage of the components, including the electronics and optics. Moreover, the system achieves matching of the optical axes of multi-transmitted laser beams, which can contribute to reducing error due to incompleteness of footprint overlap. In this paper, we evaluated the performance of airborne 1.57 µm amplitude-modulated LAS for obtaining the partial column-averaged mixing ratio of CO_2 with simultaneous range detection. In addition, the impact of integrated aerosol signals on CO_2 measurements is described in an area where aerosol was enhanced (e.g., over urban area).

2 Partial column-averaged CO_2

A LAS system on an aircraft platform was utilized for measuring the light scattered or reflected by a target (land or sea surface or thick cloud). Our system employed three narrow linewidth lasers, which are based on continuous-wave distributed feedback diode lasers and a fiber amplifier (Kameyama et al., 2011a). The system used two laser wavelengths during measurements, and the output of each laser was amplitude modulated by different sinusoidal waves. The details of amplitude modulation, frequencies, and phase shift are described in Sect. 3.

One wavelength (offline, λ_{off}), for which there was weak or no gas absorption, was selected as a reference. The other wavelength (online, λ_{on}) was selected for strong gas absorption. In this airborne test, the online wavelength could be selected from the center (λ_{center}) or edge (λ_{edge}) position of the absorption curve (as shown in Fig. 1). The online laser power was attenuated by CO_2 relative to the offline wavelength in the atmosphere. By taking the ratio of online to offline signals, we could measure $\Delta\tau$.

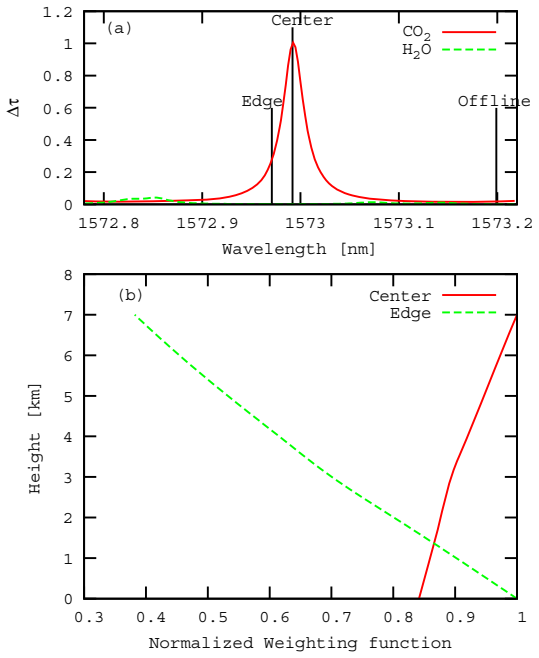

Fig. 1. (a) Operating laser wavelengths and CO_2 optical depth versus wavelength and **(b)** vertical weighting function dependent on online wavelength. Both plots were calculated using the R(12) line parameters from HITRAN 2008 and some updated data for the two-way path from the ground to an altitude of 7 km. Atmospheric parameters are based on the Air Force Geophysics Laboratory (AFGL) mid-latitude winter. CO_2 mixing ratio is assumed to be 385 ppm for all heights.

Our system obtained round-trip $\Delta\tau$ and the range (z) from the height of the aircraft above the target (Sakaizawa et al., 2010; Kameyama et al., 2011a):

$$\Delta\tau = \ln\left(\frac{P_r(\lambda_{off})}{P_r(\lambda_{on})}\frac{P_m(\lambda_{on})}{P_m(\lambda_{off})}\right) \quad (1)$$

$$z = \frac{\Delta\phi T c}{4\pi}. \quad (2)$$

In Eq. (1), $P_r(\lambda_{on})$ and $P_r(\lambda_{off})$ are the online and offline laser powers received from the surface of the ground, $P_m(\lambda_{on})$ and $P_m(\lambda_{off})$ the monitored transmitted online and offline laser powers, $\Delta\phi$ the phase difference between the monitored and the received sinusoidal signals, T the period of a modulated sinusoidal signal, and c the speed of light. The phase difference between transmitted and received sinusoidal signals corresponds to the range at which a target is acquired. Laser power is amplitude-modulated at 10 kHz for λ_{on}, and at 11 kHz for λ_{off} using $LiNbO_3$ devices. The phase identification is performed by the fast Fourier transform (FFT). This range of the detection technique is ambiguous at the inverse of the modulation frequency. However, the height of an elevated layer, such as cirrus or water clouds, can

be compared with ground returns. In addition, images taken under the moving platform help in filtering signals with cloud returns, especially over complex terrain.

The partial column-averaged dry air mixing ratio of CO_2 ($XCO_2(z)$) from the ground to the aircraft height can be described by the following equation (Ehret et al., 2008):

$$XCO_2(z_{ac}) = \Delta\tau_{ob}/2 \int_{z_{ac}}^{z_{grd}} w(r)\,dr \quad (3)$$

$$w(r) = \Delta\sigma_{CO_2}(r)\, n_{air}(r)\left(1 - V_{H_2O}(r)\right). \quad (4)$$

Here, z_{ac} is the altitude of the aircraft; z_{grd}, the height of the ground surface (mainly $z_{grd} = 0$); $w(r)$, the weighting function at a specific altitude r; $\Delta\sigma$, the differential absorption cross section of CO_2 between the online and offline wavelengths; n_{air}, the air molecular number density; and V_{H_2O}, the water vapor mixing ratio. n_{air} and V_{H_2O} are calculated from meteorological observation or mesoscale re-analysis data.

The measurement uncertainty is a quadratic summation of the precision and bias factors ($(\delta XCO_2/XCO_2)^2$ = precision^2 + bias^2). In this paper, we evaluate the precision and bias separately. The precision is evaluated using following equations:

$$\text{precision}^2 = SNR_{\Delta\tau}^{-2} + \frac{1}{W^2}\left(\frac{\partial W^2}{\partial z}\right)^2 dz^2 + \frac{1}{W^2}\left(\frac{\partial W^2}{\partial \lambda}\right)^2 d\lambda^2 \quad (5)$$

$$SNR_{\Delta\tau} = \Delta\tau/\delta\Delta\tau \quad (6)$$

$$W = \int w(r)dr \quad (7)$$

where $\delta\Delta\tau$ represents the fluctuation in measured $\Delta\tau$, and the second and third term depend on the errors of the range accuracy and the wavelength stability. If mesoscale data re-analysis is employed in Eq. (3), the error due to temporal and spatial differences compared with radiosonde measurements (corresponding to (0.16 %) ^{2}) is added to Eq. (5). Of the total error, the breakdown is as follows: 0.10 % atmospheric temperature (uncertainty of 1 K), 0.12 % atmospheric pressure (uncertainty of 1 hPa), and 0.06 % relative humidity (uncertainty of 20 %). The bias error due to surface pressure is 0.035 % (corresponding to the range measurement accuracy of 5 m).

Considering the sensitivity of near-surface CO_2 and $SNR_{\Delta\tau}$, they depend on the stabilized position of the online wavelength (Fig. 1, top panel). As shown in Table 1 and Fig. 1 (top panel), $\Delta\tau$ taken by the λ_{center} is greater than that taken by the λ_{edge}. Operation at the λ_{center} can mitigate the random error ($\delta\Delta\tau$) to decrease the required $SNR_{\Delta\tau}$. However, the weighting function of the λ_{edge} indicates a moderate peak less than an altitude of 2 km (Fig. 1, bottom panel), and yields a higher sensitivity at lower altitude. Therefore, in the case of Table 1, the difference of XCO_2 at a boundary-layer enhanced CO_2 profile is +3.9 ppm for the λ_{edge}, +2.2 ppm for the λ_{center}. This implies that the λ_{edge} can more easily indicate a contrast between urban and vegetated areas. For this purpose, the wavelength stability on λ_{edge} has to target an absolute precision of less than 1 MHz (1 SD < 300 kHz). The system with targeted wavelength stability at λ_{edge} reduces the error due to the stability of the laser wavelength less than 0.03 %. In addition, use of both edge and wing wavelength (5 GHz offset to the center wavelength) provides better surface constraint and ≥ 50 % improvement in carbon flux evaluations over vegetated land areas at ∼ 500 km resolution for spaceborne measurements (Baker et al., 2011).

Table 1. Estimated $\Delta\tau$ and sensitivity of lower altitude CO_2 for the center and edge wavelength. Atmospheric parameters are based on the AFGL mid-latitude winter. Two CO_2 vertical profiles (boundary-layer enhanced and constant along height) were assumed: for one, the CO_2 mixing ratio was constant at 385 ppm along height; for the other, the mixing ratio was 410 ppm from the ground to 0.5 km, 398 ppm from an altitude of 0.5 to 2 km, and 385 ppm at an altitude above 2 km altitude, respectively.

	385 ppm constant		Urban area	
	Center	Edge	Center	Edge
$\Delta\tau$ at 7 km	0.970	0.261	0.975	0.266
XCO_2 at 7 km	385.0	385.0	387.2	398.9

The bias error is evaluated from the impact of the elevated particulate layer on the measured bias (τ_{bias}) and the spectroscopic parameter. The bias factor due to spectroscopic parameters is calculated using the Voigt profile function and the uncertainty from earlier studies (Devi et al., 2007; Rothman et al., 2009; Predoi-Cross et al., 2009). Measured τ_{bias} is related to the path-integrated intensity of the aerosol layer or cirrus clouds. A narrow field of view and employment of range detection can allow ground and cloud return signals to be distinguished. Assuming the backscatter coefficients of suburban aerosol data (Sakaizawa et al., 2009), we found that the bias from the integrated backscatter depends on the surface albedo, for example, 0.13 % for a surface albedo of 0.1 sr^{-1} and 0.05 % for an albedo of 0.3 sr^{-1}. This evaluation indicates that higher surface albedo (such as for deserts) can suppress the impact of path-integrated aerosol intensity. Mitigation due to amplitude modulation is described in more detail in Kameyama et al. (2011b).

3 Airborne instruments

We first manufactured an LAS system for ground-based measurements (Kameyama et al., 2011a; Sakaizawa et al., 2009). Figure 2 shows the block diagram of the 1.57 µm prototype LAS system and other instrument settings in the aircraft cabin. The specifications for the instruments are summarized in Table 2.

The online and offline sources were polarization-maintained, fiber-coupled diode lasers. The other system is based on optical fiber circuits. Laser-1 (as the center of

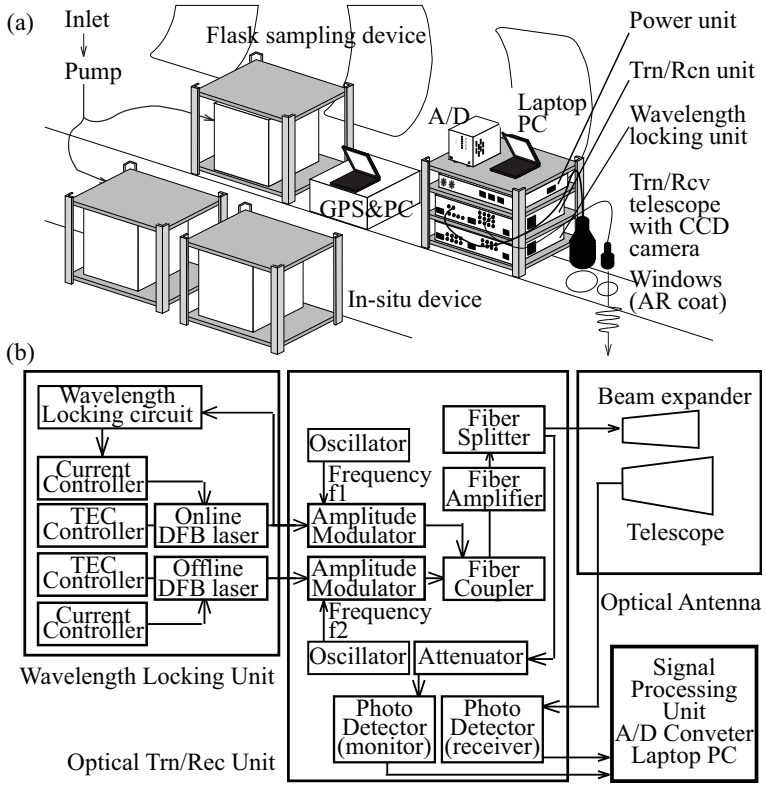

Fig. 2. (a) Airborne instrument setup and **(b)** block diagram of the 1.57 µm prototype LAS system. TEC: thermoelectric cooler, DFB laser: distributed feedback laser. Trn/Rcv: Transmitting/Receiving.

online wavelength) was stabilized within a root-mean-square (RMS) value of 12 MHz at the peak of the R(12) line in the $30012 \leftarrow 00001$ absorption band using a gas cell filled with pure CO_2 instead of the reference cavity used in the Pound–Drever–Hall method (Drever et al., 1983). The gas cell was sealed with a gas pressure of 0.1 atm. Laser-2 (as the edge of online wavelength) was stabilized at a position of 2.55 GHz offset from the center position. Laser-1 and Laser-2 were combined using a fiber combiner and detected using a photodiode (InGaAs-PD). The PD generates a heterodyne signal in which the beat signal was controlled at a constant 2.55 GHz. Laser-3 was stabilized at offline wavelength within 48 MHz RMS by controlling its temperature and injection currents. The fiber-coupled outputs were amplitude modulated with $LiNbO_3$ devices. Each modulation signal had a different sinusoidal frequency. The modulated outputs were combined and amplified using a fiber amplifier. Almost all of the amplified power (99 %) was expanded and transmitted through an anti-reflection coated window. The diameter of the transmitted $1/e^2$ beam was 60 mm, and the full angle beam divergence was 0.12 mrad. The total transmitted power at the fiber end was 1.2 W. The residual 1 % was monitored as a reference for received signals. Scattered signals from the ground surface were collected using a receiving telescope with a field of view of 0.2 mrad and a 110 mm active aperture. The receiving and transmitting optics were fixed on a rigid base plate. The signals were focused on a multi-mode fiber with a 200 µm core diameter and detected using a 0.5 mm diameter InGaAs-PIN PD. The received signals were digitized using a high-speed digitizer (60 MS s^{-1}, 14 bit). The wavelength identification and power evaluation were performed by means of fast Fourier transform (FFT) on a laptop computer.

Airborne in situ CO_2 measurements were carried out using a module consisting of a commercial CO_2 analyzer (LI-COR, Inc., Type: LI-840) modified for airborne operation (Machida et al., 2008). In addition, other trace gases, such as carbon monoxide, methane, etc., were also determined by air analysis using flask sampling devices. Both systems collected air from outside the aircraft using stainless steel sampling tubes facing the direction of flight. The flask sampling was only performed during spiral flights. The time resolution of the in situ data was 2 s. The precision of in situ measurements was 0.12 ppm (1 SD) in 2 s data. The end-to-end performance was additionally affected by a change in the instrumental stability. Consequently, highly accurate calibrated gases were used to compensate the instrumental drift. Hence, the total uncertainty of the in situ CO_2 measurement was estimated within ± 0.5 ppm.

Table 2. Specifications for instrumental and spectroscopic data.

Transmitter	
Online (cm^{-1})	6357.31113
Offline (cm^{-1})	6356.49917
Transmitter power (W)	1.2 (Fiber end)
Frequency stability (MHz)	On: 12, Off: 48
Modulation frequency (kHz)	On: 10, Off: 11
Beam diameter (mm)	60
Beam divergence (mrad)	0.12
FWHM of laser linewidth (MHz)	0.8
Receiver	
Receiver diameter (mm)	110
FOV (mrad)	0.2
Detector	InGaAs-PIN
Bandwidth (kHz)	200
Detector size (µm)	200
Distinguish on/off	FFT
Integration time (s)	2
A/D speed ($MS\,s^{-1}$)	1
A/D resolution (bit)	14
Spectroscopic data*	
Center wavenumber (cm^{-1})	6357.31157
Line intensity ($cm^{-1}\,molec^{-1}\,cm^2$)	1.6613×10^{-23}
Air-broadening coeff. ($cm^{-1}\,atm^{-1}$)	0.07781
Air-pressure shift coeff. ($cm^{-1}\,atm^{-1}$)	-4.30×10^{-3}
Self-pressure shift coeff. ($cm^{-1}\,atm^{-1}$)	-4.82×10^{-3}
Temperature index for broadening coeff.	0.695
Lower state energy (cm^{-1})	60.8709

* Rothman et al. (2009), Devi et al. (2007), and Predoi-Cross et al. (2009)

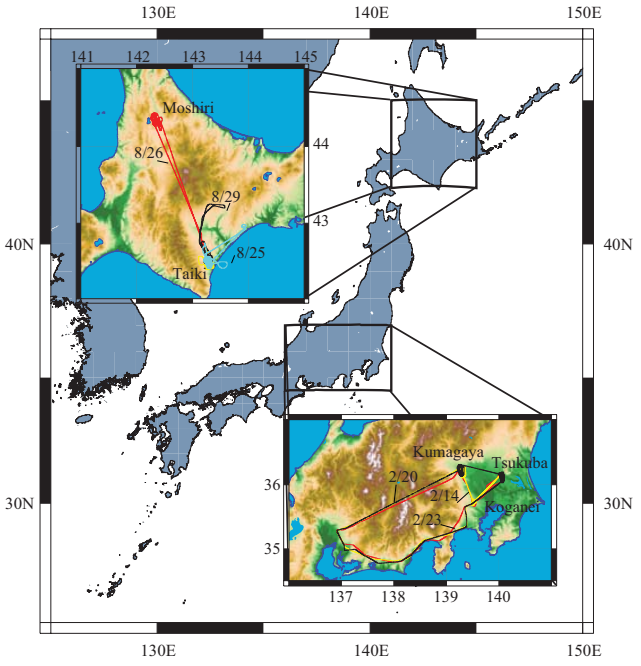

Fig. 3. Flight paths of the aircraft measurements in August 2009 (top panel) and February 2010 (bottom panel).

4 Experiment

Nine flights were conducted for evaluating the value of $XCO_2(z)$ during August 2009 and February 2010. The aircraft used was a Beechcraft King Air (Type: 200T, operated by Diamond Air Service Inc.), and each flight lasted approximately 4 h, including the spiral and level flights. These flights were performed under various conditions, such as over the land and sea, in clear skies, and on partial cloudy days. The flight paths taken are depicted in Fig. 3.

The measurements in August were taken over Hokkaido prefecture in northern Japan, while those in February were taken over the Tsukuba and Koganei sites. The Tsukuba site is approximately 50 km northeast, and the Koganei site is approximately 10 km west of the center of Tokyo. The LAS system provides the $\Delta\tau$ and the range from the aircraft to the target. The amplitude modulation frequencies were 10 kHz for the online wavelength and 11 kHz for the offline wavelength in this measurement. The transmitting online wavelength was set to the edge position of absorption in August 2009 (as shown in Fig. 1), and the center position was used as the online wavelength in February 2010. The accumulation time was 2 s during both measurements. An additional 3 s were required for signal processing on the laptop computer. A visible CCD camera (ARTRAY Inc., Model ARTCAM 150pIII) also monitored the landscape under the aircraft every 5 s. These temporal images were capable of detecting cloud cover over both land and sea.

To validate the LAS measurements, atmospheric CO_2 was taken from 1500 ft (0.5 km) to 23 500 ft (7 km) using flask sampling and in situ CO_2 devices. Simultaneous radiosonde measurements were carried out by the Japan Weather Agency under a contract with the National Institute for Environmental Studies during the spiral flight measurements over the Moshiri site (Hokkaido) in August and the Tsukuba site in February. Other radiosonde measurements at the Koganei site, corresponding to the path of the aircraft, were also performed by the National Institute of Information Communications Technology. Spiral flight measurements were taken over the Tsukuba (0.5 to 2 km) and Koganei (0.5 to 3 km) sites owing to air traffic control regulations. We employed flask sampling data for validation in August, as the in situ data were unusable owing to a gas leak in the instrument.

5 Results

Figure 4 graphically illustrates the return signal intensity for the August and February measurements. Various return signals were obtained over grassland, urban areas, and the surface of the sea. The return signals were consistent with z^{-2}. Both offline signals were attenuated by weak CO_2 absorption

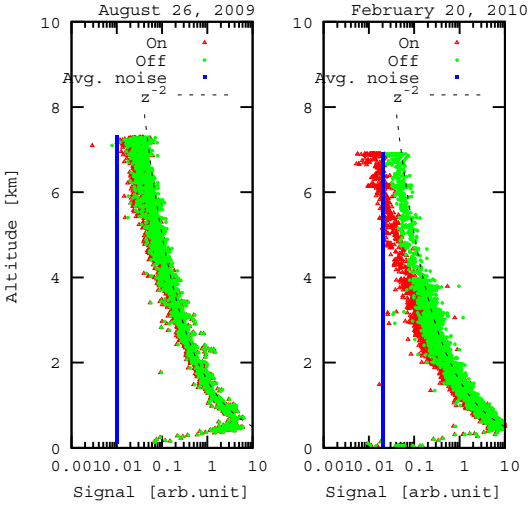

Fig. 4. Received return signals at various elevations in August 2009 (left panel) and February 2010 (right panel). Triangle (△): online signal; circle (◯): offline signal; square (□): averaged noise level; dashed curve: z^{-2}. The edge and center online wavelengths (Fig. 1) were used in August 2009 and February 2010, respectively.

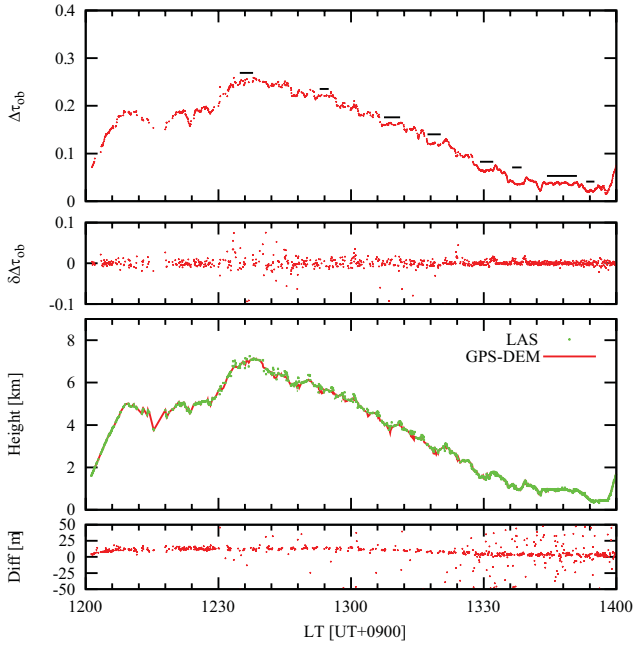

Fig. 5. Results of airborne flight measurements taken on 26 August 2009. The upper two panels show the differential absorption optical depth ($\Delta\tau$) and its fluctuations versus time, and the lower two panels represent the heights and their differences obtained from LAS and airborne GPS and DEM. The LAS measurement was carried out with cloud screening. XCO_2 is calculated from averaged $\Delta\tau$ indicated by solid line in the top panel. The measured data from the LAS were corrected according to the information flight attitude. However, some peaks at $\Delta\tau$ and aircraft height resulted from imperfect correction of the viewing angle.

regardless of observation sites. It is clear that CO_2 differential absorption strength varies according to the position of the online wavelength.

Figures 5 and 6 show the temporal $\Delta\tau$, its fluctuations, and the range from the aircraft to the targets. The graphs at the top of Figs. 5 and 6 depict $\Delta\tau$, while the graphs immediately below it (in both figures) depict $\delta\Delta\tau$. The third graphs from the top depict the optical path length from LAS, the geometrical height from airborne GPS, and the digital elevation model (DEM) from ASTER (Yamaguchi et al., 1998). The graphs at the bottom illustrate the difference between the range obtained from LAS and the geometrical height. The aircraft altitudes from the LAS are corrected according to the information of flight attitude. However, some peaks at $\Delta\tau$ and aircraft altitude resulted from imperfect correction of the viewing angle. These uncorrected data are excluded when the altitude accuracy and XCO_2 are evaluated. The spiral flight measurements in August 2009 was taken over the Moshiri site (basin in a mountainous area, rough field). Meteorological data from radiosonde were obtained over the Moshiri site. The results in February 2010 also included two sets of spiral measurements over the Tsukuba site. Simultaneous radiosonde measurements were also taken.

The values of $SNR_{\Delta\tau}$ at an altitude of 2 km were 147 in August and 270 in February. The corresponding errors due to the value of $\delta\Delta\tau$ were 0.68 % ($2\,\Delta\tau = 0.18$) in August and 0.37 % ($2\,\Delta\tau = 0.54$) in February. The error at an altitude of 7 km was 0.85 % ($2\,\Delta\tau = 0.51$, $SNR_{\Delta\tau} = 118$) in August. It was found that the $SNR_{\Delta\tau}$ in February (2 km altitude) was 2.5 times greater than that in August (7 km altitude), despite the fact that $\Delta\tau$ was nearly unity. This resulted from attenuated return signal intensities from more distant targets. As illustrated in Fig. 4, the return signals at 7 km altitude in August were smaller than those obtained at a 2 km altitude in February. Furthermore, when $\Delta\tau$ is small, it is associated with significant online fluctuation at the edge position. The error due to fluctuation of the operating wavelength ($\partial \int w\,dr/\partial\lambda$) was evaluated as being less than 0.58 % at the edge of the online wavelength and 0.05 % at its center. These errors can be reduced by optimizing transmitted laser power, receiving aperture, and detector dark current noise. These improvements result in more precise measurement with more shorter integration time.

To validate LAS altitude, we extracted the geometric height from the on-board GPS and the ASTER-GDEM. Cloud screening was performed in August. The resolution of the DEM was approximately 30 m per pixel, 7–14 m (= 1 SD) vertical precision over a flat field, and 20–30 m over complex terrain, such as mountain slopes (Hirano et al., 2003). The altitude of the aircraft obtained from LAS was consistent with that from GPS-DEM: the difference between the LAS and geometric heights was less than ± 15 m (1 SD = 4.9 m) over a flat field and ± 15–30 m during rotating movements. The

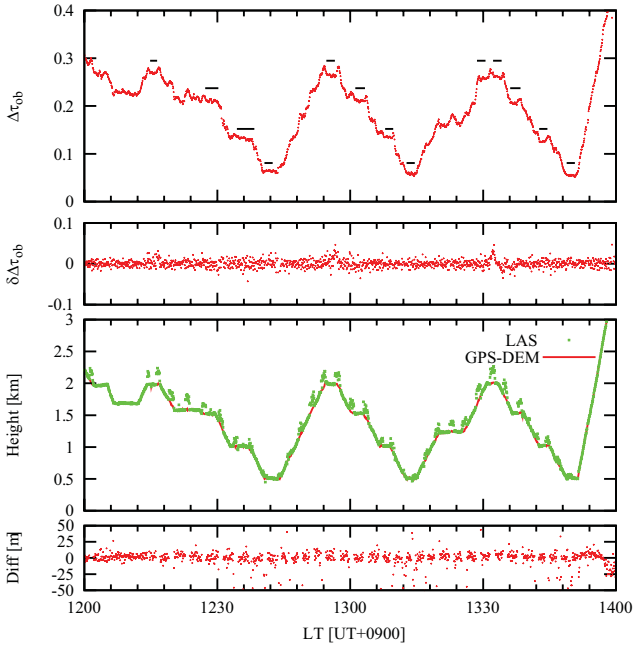

Fig. 6. Results of airborne flight measurements taken on 23 February 2010. These data were taken over the Tsukuba site (urban area). Some data points that lie off the validation data resulted from imperfect correction of the viewing angle. These uncorrected data are excluded when the altitude accuracy and XCO_2 are evaluated.

precision of the range measurement and the accuracy of the ground-based measurements were confirmed as 2 and 5 m, respectively (Sakaizawa et al., 2010). The measured phase difference when calculating the target range was based on averaged return signals coming from groups of trees, buildings, and ground surface over a range from 150 to 200 m in these airborne measurements. The probability of detecting elevations from ground surfaces varies because of the presence of trees over the integration range, and the effective optical path also changes during rotating movement, which may be sources of potential bias in measured mean aircraft altitude. The error due to range measurement ($\partial \int w\,\mathrm{d}r/\partial z$) was 0.12 %. The bias error due to the Voigt profile using the spectroscopic data for the CO_2 R(12) line was estimated to be 0.13 %; the spectroscopic data were taken from recent studies (Devi et al., 2007; Rothman et al., 2009; Predoi-Cross et al., 2009).

$\Delta\tau$ was compared with validation data ($\Delta\tau_{\mathrm{val}}$) calculated from CO_2 concentrations from 1500 ft (0.5 km) to 23 500 ft (7 km). The values of CO_2 concentrations are collected through the airborne in situ or flask sampling devices shown in Fig. 7. $\Delta\tau_{\mathrm{val}}$ can be evaluated using the following equation:

$$\Delta\tau_{\mathrm{val}} = \int_{z_{\mathrm{ac}}}^{z_{\mathrm{grd}}} n_{\mathrm{CO_2}}(r)\, w(r)\, \mathrm{d}r \qquad (8)$$

Table 3. Partial column-averaged CO_2 from the ground to airplane height and aerosol optical depth from the 0.5 to 2 km (February 2010).

	14 Feb	20 Feb	23 Feb
z^* [m]	1966	1925	1973
Aerosol OD	0.11	0.07	0.12
XCO_{2LAS} (1 SD**)	398.7 (2.4)	398.8 (2.3)	400.6 (2.4)
XCO_{2val}	397.41	397.36	398.85

* z is the airplane height. ** 1 SD means measurement precision.

where $n_{\mathrm{CO_2}}(r)$ is the dry air mixing ratio from the flask sampling or in situ $n_{\mathrm{CO_2}}$ data. The CO_2 profiles ($n_{\mathrm{CO_2}}(r)$) are calculated with a third-order polynomial fitting. The CO_2 concentration from the ground to an altitude of 0.5 km was assumed to be constant, due to a lack of surface CO_2 measurements. Figure 8 indicates the linear relation between XCO_{2LAS} and XCO_{2val} over the urban area. Note that XCO_{2LAS} and XCO_{2val} are in agreement, as their correlation coefficient (R) is 0.987 for XCO_2, 0.995 for $\Delta\tau$. The difference of XCO_{2LAS} to XCO_{2val} is a negative bias of 1.5 ppm with 1 SD = 2.4 ppm. The negative bias between XCO_{2LAS} and XCO_{2val} may be attributed to bias sources due to aerosol return signals from nearest area less than 500 m from the aircraft (the overlapping function between fields of view of receiving optics and transmitting laser beam becomes unity after 500 m), the impact of signal averaging over structured terrain (corresponding to range accuracy), and spectroscopic parameters.

The graph on the left in Fig. 9 indicates XCO_{2LAS} from the ground to various elevations, while the graph on the right indicates the difference between the validation data (in situ and flask sampling) and the measured data. The results indicate a maximum difference of 4 ppm and an averaged difference of 1.5 ppm. XCO_{2LAS} for the August measurements shows lower CO_2 levels below 2 km than above 2 km, as seen in the in situ data in Fig. 7a. XCO_{2LAS} for the February measurements shows the boundary-layer enhanced CO_2 (as shown in Fig. 7b–e) and a tendency to decrease monotonically with height. Note that the August measurements were impacted by photosynthesis in the biosphere, while the February measurements were impacted by a high CO_2 mixing ratio.

We evaluated the impact of distributed aerosol on spaceborne CO_2 measurement and found that the bias was less than 0.27 %, as described in Kameyama et al. (2011b). The effect of the other bias factors was evaluated as 0.13 % due to spectroscopic parameters and 0.12 % due to structured terrain (corresponding to range measurement accuracy). The total bias error (τ_{bias}) is at least 0.52 %, which is reasonable compared with the difference between XCO_{2LAS} and XCO_{2val}.

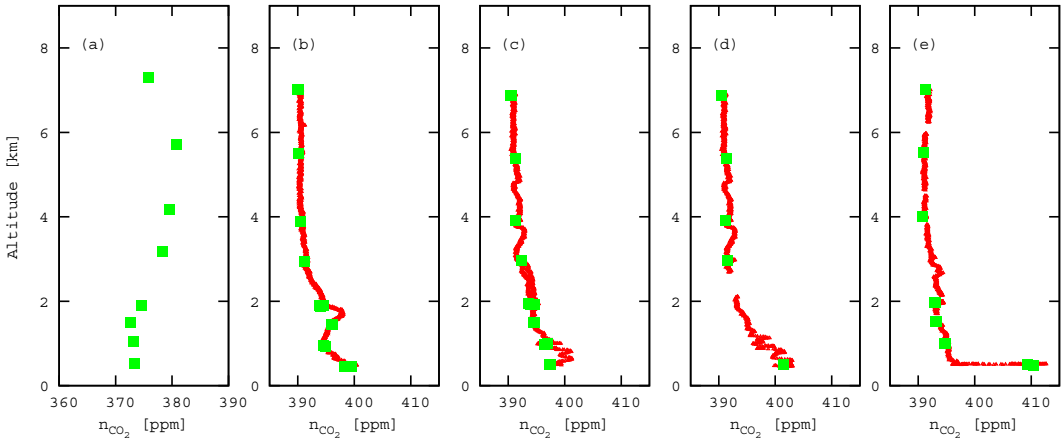

Fig. 7. Atmospheric CO_2 profiles from airborne flask (green squares) and in situ devices (red points). **(a)** 26 August 2009, taken over Moshiri (0–7 km); **(b)** 14 February 2010; and **(c)** 20 February 2010, over Kumagaya (2–7 km) and Tsukuba (0.5–2 km); **(d)** 20 February 2010 over Kumagaya (2–7 km) and Koganei (0.5–3 km); **(e)** 23 February 2010, over Kumagaya (2–7 km) and Tsukuba (0.5–2 km).

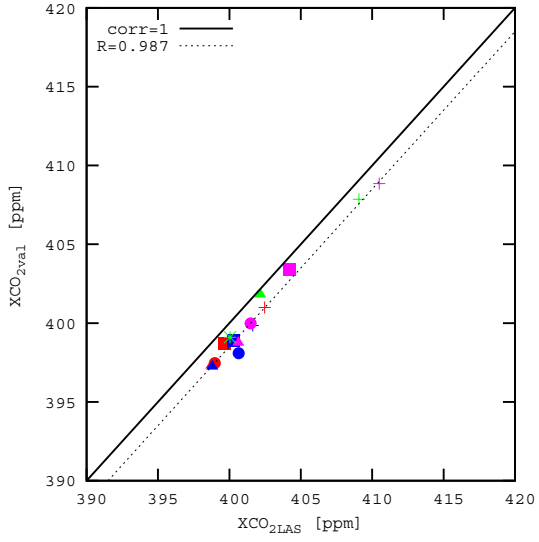

Fig. 8. Correlation between measured and calculated XCO_2 from the ground to the aircraft height. Asterisk (∗): 10 000 ft, triangle (△): 6500 ft; circle (◯): 5000 ft; square (□): 3300 ft; cross point (+): 1600 ft. Red: 14 February (Tsukuba); Green: 14 February (Koganei); Blue: 20 February (Tsukuba); Purple: 23 February (Tsukuba).

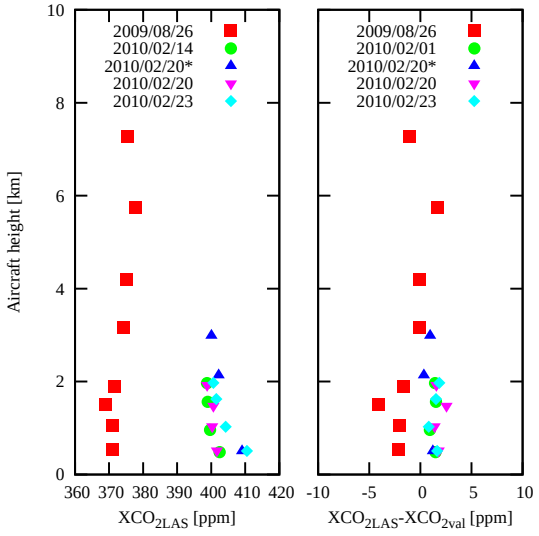

Fig. 9. Evaluated partial column-averaged column CO_2 (XCO_{2LAS}) obtained from LAS (left panel) and the difference compared with calculated values (XCO_{2val}) from flask and in situ measurements (right panel).

In the case of the Tsukuba site, aerosol distributions were measured using a 532-nm ground-based LIDAR. We could not use data analysis of aerosol distribution at other sites, but the atmosphere above Moshiri site is generally clear compared with an urban area such as Tsukuba site. The aerosol optical depth (AOD) from an altitude of 0.4 to 2 km was also evaluated from the LIDAR data. Values of AOD were found to be 0.11 on 14 February, 0.07 on 20 February and 0.12 on 23 February during airborne measurements, for which the corresponding XCO_{2LAS} and XCO_{2val} at an altitude of 2 km are summarized in Table 3. The difference of XCO_{2LAS} to XCO_{2val} is −1.5 ppm, and evaluated XCO_{2LAS} is in agreement with XCO_{2val} within the measurement precision of 2.4 ppm (1 SD); nevertheless, not only CO_2 concentrations but also aerosols are highly distributed in the lower atmosphere.

The global distribution of AOD values, obtained from space-borne measurements by extraction from the 5 km mesh of the CALIPSO level 2 aerosol layer through the year 2008, ranges from 0.02 to 2. The AOD range without any thick clouds indicated that AOD values of less than 0.12 account for 72 % of the total observed data, while AOD values of

less than 0.2 account for more than 84 %. The XCO_{2LAS} measurements listed in Table 3 were observed under the above probability for column-integrated AOD, for which the corresponding AOD at 532 nm is partial column-integrated. In addition, the error is considerably smaller than in the case of the airborne measurement where the modulation frequency is higher than 30 kHz (Kameyama et al., 2011b).

6 Conclusions

We demonstrated an airborne measurement system for simultaneous detection of the column-averaged dry air mixing ratio of CO_2 ($XCO_2(z)$) and target range using a 1.57-µm laser absorption spectrometer. The observed partial column-averaged dry air mixing ratio and validation data were in good agreement and showed a high correlation coefficient (R) of 0.987. The difference between the value of XCO_{2LAS} and the validation data XCO_{2val} had a maximum value of 4 ppm and an average value of 1.5 ppm. In the dense aerosol environment over urban area, the values of XCO_{2LAS} and XCO_{2val} were in agreement within the measurement precision of 2.4 ppm, with the corresponding aerosol optical depth in the range 0.07–0.12. In addition, the observed $XCO_2(z)$ profiles indicated a significant similarity to the validation data. Even though LAS employed a small effective aperture and had a low transmitting laser power, a precision better than 1 % for simultaneous measurements of CO_2 and altitude could be demonstrated. Our prototype LAS, which is engineering designed, will serve as a base for a near-future spaceborne system.

Acknowledgements. We would like to thank T. Machida and his research group from the National Institute for Environmental Studies, Ibaraki, Japan, for their analysis of the flask data. We would also like to say a special thank you to Y. Miyamoto from the Graduate School of Natural Science and Technology, Okayama University, Okayama, Japan. We would like to thank K. Mizutani and S. Ishii of NICT, Tokyo, Japan, for providing radiosonde data to calculate the column-averaged mixing ratio of CO_2. H. Ohyama of JAXA, Ibaraki, Japan, gave insightful support for error evaluation. We are grateful to T. Nagai and T. Sakai of the Meteorological Research Institute, Ibaraki, Japan, for the aerosol LIDAR data analysis. ASTER GDEM is a product of METI and NASA.

Edited by: W. R. Simpson

References

Abshire, J. B., Riris, H., Allan, G. R., Weaver, C. J., Mao, J., Sun, X., Hasselbrack, W. E., Kawa, S. R., and Biraud, S.: Pulsed airborne lidar measurement of atmospheric CO_2 column absorption, Tellus B, 52, 770–783, doi:10.1111/j.1600-0889.2010.00502.x, 2010.

Amediek, A., Fix, A., Wirth, M., and Ehret, G.: Development of an OPO system at 1.57 µm for integrated path DIAL measurement of atmospheric carbon dioxide, Appl. Phys. B, 92, 295–302, doi:10.1007/s00340-008-3075-6, 2008.

Baker, D. F., Kawa, S. R., Rayner, P. J., Browell, E. V., Menzies, R. T., and Abshire, J. B.: CO_2 Flux Inversion Error Analyses for Future Active Space CO_2 Missions like ASCENDS, AGU General Assembly, 5–9 December 2011, AGU2011-AC34C-02, San Francisco, USA, 2011.

Browell, E. V., Dobler, J., Kooi, S. A., Choi, Y., Harrison, F. W., Moore, B., and Zaccheo, T. S.: Airborne Validation of Laser Remote Measurements of Atmospheric Carbon Dioxide, AGU General Assembly, 5–9 December 2011, AGU2011-A34C-04, San Francisco, USA, 2011.

Devi, V. M., Benner, D. C., Brown, L. R., Miller, C. E., and Toth, R. A.: Line mixing and speed dependence in CO_2 at 6227.9 cm^{-1}: constrained multispectrum analysis of intensities and line shapes in the 30013 ← 00001 band, J. Mol. Spectrosc., 245, 52–80, doi:10.1016/j.jms.2007.05.015, 2007.

Drever, R., Hall, J., Kowalski, F., Hough, J., Ford, G., Munley, A., and Ward, H.: Laser phase and frequency stabilization using an optical resonator, Appl. Phys. B, 31, 97–105, doi:10.1007/BF00702605, 1983.

Ehret, G., Liemle, C., Wirth, M., Amediek, A., Fix, A., and Houweling, S.: Space-borne remote sensing of CO_2, CH_4, and N_2O by integrated path differential absorption lidar: a sensitivity analysis, Appl. Phys. B, 90, 593–608, doi:10.1007/s00340-007-2892-3, 2008.

Gibert, F., Koch, G., Davis, K. J., Beyon, J. Y., Hilton, T., Andrews, A., Flamant, P., and Singh, U. N.: Can CO_2 turbulent flux be measured by lidar? A preliminary study, J. Atmos. Ocean. Tech., 28, 365–377, doi:10.1175/2008JTECHA1070.1, 2011.

Hirano, A., Welch, R., and Lang, H.: Mapping from ASTER stereo image data: DEM validation and accuracy assessment, ISPRS J. Photogramm., 57, 356–370, doi:10.1016/S0924-2716(02)00164-8, 2003.

Houweling, S., Breon, F.-M., Aben, I., Rödenbeck, C., Gloor, M., Heimann, M., and Ciais, P.: Inverse modeling of CO_2 sources and sinks using satellite data: a synthetic inter-comparison of measurement techniques and their performance as a function of space and time, Atmos. Chem. Phys., 4, 523–538, doi:10.5194/acp-4-523-2004, 2004.

IPCC 2007: Summary for policymakers, in: Climate Change 2007, The Physical Science Basis, Contribution of Working Group I to the Fourth Assessment Report of the Intergovernmental Panel on Climate Change, edited by: Solomon, S., Qin, D., Manning, M., Chen, Z., Marquis, M., Averyt, K. B., Tignor, M., and Miller, H. L., Cambridge University Press, Cambridge, UK and New York, NY, USA.

Ishii, S., Mizutani, K., Fukuoka, H., Ishikawa, T., Philippe, B., Iwai, H., Aoki, T., Itabe, T., Sato, A., and Asai, K.: Coherent 2 µm differential absorption and wind lidar with conductively cooled laser and two-axis scanning device, Appl. Optics, 49, 1809–1817, doi:10.1364/AO.49.001809, 2010.

Kameyama, S., Imaki, M., Hirano, Y., Ueno, S., Kawakami, S., Sakaizawa, D., and Nakajima, M.: Performance improvement and analysis of a 1.6 µm continuous-wave modulation laser absorption spectrometer system for CO_2 sensing, Appl. Optics, 50, 1560–1569, doi:10.1364/AO.50.001560, 2011a.

Kameyama, S., Imaki, M., Hirano, Y., Ueno, S., Kawakami, S., Sakaizawa, D., Kimura, T., and Nakajima, M.: Feasibility study on 1.6 µm continuous-wave modulation laser absorption spectrometer system for measurement of global CO_2 concentration from a satellite, Appl. Optics, 50, 2055–2068, doi:10.1364/AO.50.002055, 2011b.

Kaminske, T., Scholze, M., and Houweling, S.: Quantifying the benefit of A-SCOPE data for reducing uncertainties in terrestrial carbon fluxes in CCDAS, Tellus B, 52, 784–796, doi:10.1111/j.1600-0889.2010.00483.x, 2010.

Kawa, S. R., Mao, J., Abshire, J. B., Collatz, G. J., Sun, X., and Weaver, C. J.: Simulation studies for a space-based CO_2 lidar mission, Tellus B, 52, 759–769, doi:10.1111/j.1600-0889.2010.00486.x, 2010.

Kuze, A., Suto, H., Nakajima, M., and Hamazaki, T.: Thermal and near infrared sensor for carbon observation Fourier-transform spectrometer on the greenhouse gases observing satellite for greenhouse gases monitoring, Appl. Optics, 48, 6716–6733, doi:10.1364/AO.48.006716, 2009.

Machida, T., Matsueda, H., Sawa, Y., Nakagawa, Y., Hirotani, K., Kondo, N., Goto, K., Nakazawa, T., Ishikawa, K., and Ogawa, T.: Worldwide measurements of atmospheric CO_2 and other trace gas species using commercial airlines, J. Atmos. Ocean. Tech., 25, 1744–1754, doi:10.1175/2008JTECHA1082.1, 2008.

Makshutov, S., Patra, P. K., Onishi, R., Saeki, T., and Nakazawa, T.: NIES/FRCGC Global Atmospheric Tracer Transport Model: Description, Validation, and Sources and Sinks Inversion, J. Earth Sim., 9, 3–18, 2008.

Miller, C. E., Crisp, D., DeCola, P. L., Olsen, S. C., Randerson, J. T., Michalak, A. M., Alkhaled, A., Rayner, P., Jacob, D. J., Suntharalingam, P., Jones, D. B. A., Denning, A. S., Nicholls, M. E., Doney, S. C., Pawson, S., Boesch, H., Connor, B. J., Fung, I. Y., O'Brien, D., Salawitch, R. J., Sander, S. P., Sen, B., Tans, P., Toon, G. C., Wennberg, P. O., Wofsy, S. C., Yung, Y. L., and Law, R. M.: Precision requirements for space-based X_{CO_2} data, J. Geophys. Res., 112, D10314, doi:10.1029/2006JD007659, 2007.

Morino, I., Uchino, O., Inoue, M., Yoshida, Y., Yokota, T., Wennberg, P. O., Toon, G. C., Wunch, D., Roehl, C. M., Notholt, J., Warneke, T., Messerschmidt, J., Griffith, D. W. T., Deutscher, N. M., Sherlock, V., Connor, B., Robinson, J., Sussmann, R., and Rettinger, M.: Preliminary validation of column-averaged volume mixing ratios of carbon dioxide and methane retrieved from GOSAT short-wavelength infrared spectra, Atmos. Meas. Tech., 4, 1061–1076, doi:10.5194/amt-4-1061-2011, 2011.

Palmer, P. I., Feng, L., and Bösch, H.: Spatial resolution of tropical terrestrial CO_2 fluxes inferred using space-borne column CO_2 sampled in different earth orbits: the role of spatial error correlations, Atmos. Meas. Tech., 4, 1995–2006, doi:10.5194/amt-4-1995-2011, 2011.

Predoi-Cross, A., McKellar, A., Benner, D., Devi, V. M., Gamache, R., Miller, C. E., Toth, R. A., and Brown, L. R.: Temperature dependences for air-broadened Lorentz half-width and pressure shift coefficients in the $30013 \leftarrow 00001$ and $30012 \leftarrow 00001$ bands of CO_2 near 1600 nm, Can. J. Phys., 87, 517–535, doi:10.1139/P08-137, 2009.

Randall, D. A., Wood, R. A., Bony, S., Colman, R., Fichefet, T., Fyfe, J., Kattsov, V., Pitman, A., Shukla, J., Srinivasan, J., Stouffer, R. J., Sumi, A., and Taylor, K. E.: Climate models and their evaluation, in: Climate Change 2007: The Physical Science Basis, Contribution of Working Group I to the Fourth Assessment Report of the Intergovernmental Panel on Climate Change, edited by: Solomon, S., Qin, D., Manning, M., Chen, Z., Marquis, M., Averyt, K. B., Tignor, M., and Miller, H. L., Cambridge University Press, Cambridge, UK and New York, NY, USA.

Rayner, P. J. and O'Brien, D. M.: The utility of remotely sensed CO_2 concentration data in surface source inversions, Geophys. Res. Lett., 28, 175–178, 2001.

Rothman, L. S., Gordon, I. E., Barbe, A., Benner, D. C., Bernath, P. F., Birk, M., Boudonf, V., Brown, L. R., Champargue, A., Champion, A., Chance, A., Coudert, L. H., Dana, V., Devi, V. M., Fallyk, S., Flaud, J.-M., Gamache, R. R., Goldman, A., Jacquemart, D., Kleiner, I., Lacome, N., Lafferty, W. J., Mandin, J.-Y., Massie, S. T., Mikhailenko, S. N., Miller, C. E., Moazzen-Ahmad, N., Naumenko, O. V., Nikitin, A. V., Orphal, J., Perevalov, V. I., Perrin, A., Predoi-Cross, A., Rinsland, C. P., Rotger, M., Simeckova, M., Smith, M. A. H., Sung, K., Tashkun, S. A., Tennyson, J., Toth, R. A., Vandaelev, A. C., and Auweka, J. V.: The HITRAN 2008 molecular spectroscopic database, J. Quant. Spectrosc. Ra., 110, 533–572, doi:10.1016/j.jqsrt.2009.02.013, 2009.

Sakaizawa, D., Nagasawa, C., Nagai, T., Abo, M., Shibata, Y., Nakazato, M., and Sakai, T.: Development of a 1.6 µm differential absorption lidar with a quasi-phase matching OPO and photon-counting detector for the vertical CO_2 profile, Appl. Optics, 48, 748–757, doi:10.1364/AO.48.000748, 2009.

Sakaizawa, D., Kawakami, S., Nakajima, M., Sawa, Y., and Matsueda, H.: Ground-based demonstration of a CO_2 remote sensor using a 1.57 µm differential laser absorption spectrometer with direct detection, J. Appl. Remote Sens., 4, 043548, doi:10.1117/1.3507092, 2010.

Spiers, G. D., Menzies, R. T., Jacob, J., Christensen, L. E., Phillips, M. W., Choi, Y., and Browell, E. V.: Atmospheric CO_2 measurements with a 2 µm airborne laser absorption spectrometer employing coherent detection, Appl. Optics, 50, 2098–2111, doi:10.1364/AO.50.002098, 2011.

Yamaguchi, Y., Kahle, A. B., Tsu, H., Kawakami, T., and Pniel, M.: Overview of Advanced Spaceborne Thermal Emission and Reflection Radiometer (ASTER), IEEE T. Geosci. Remote, 36, 1062–1071, doi:10.1109/36.700991, 1998.

Yoshida, Y., Ota, Y., Eguchi, N., Kikuchi, N., Nobuta, K., Tran, H., Morino, I., and Yokota, T.: Retrieval algorithm for CO_2 and CH_4 column abundances from short-wavelength infrared spectral observations by the Greenhouse gases observing satellite, Atmos. Meas. Tech., 4, 717–734, doi:10.5194/amt-4-717-2011, 2011.

Yu, J., Braud, A., and Petros, M.: 600-mJ double-pulse 2 µm laser, Opt. Lett., 28, 540–542, doi:10.1364/OL.28.000540, 2003.